Applied Surface Science 286 (2013) 344–350

Contents lists available at ScienceDirect

Applied Surface Science

journal homepage: www.elsevier.com/locate/apsusc

A spontaneous dissolution approach to carbon coated TiO_2 hollow composite spheres with enhanced visible photocatalytic performance

Zewu Zhang, Yuming Zhou*, Yiwei Zhang, Xiaoli Sheng, Shijian Zhou, Sanming Xiang

School of Chemistry and Chemical Engineering, Southeast University, Nanjing 211189, PR China

ARTICLE INFO

Article history:
Received 16 July 2013
Received in revised form
12 September 2013
Accepted 15 September 2013
Available online 21 September 2013

Keywords:
TiO_2–carbon
Hollow spheres
Spontaneous dissolution
Visible-light photodegradation

ABSTRACT

TiO_2/carbon hollow composite spheres with mesoporous structure were successfully prepared by using a conventional hard template method but without an on-purpose etching process to remove the core material. A possible surface-protected dissolution mechanism was proposed to account for the spontaneous dissolution of the silica core. The thickness of carbon layer could be well controlled by adjusting the concentration of glucose in the hydrothermal reaction. Moreover, the as-prepared TiO_2/C hollow spheres had remarkable light absorption in the visible region. As compared with the SiO_2@TiO_2 solid spheres prepared without the addition of glucose, the TiO_2/C hollow spheres exhibited enhanced photocatalytic efficiency for the visible-light photodegradation of Rhodamine B.

1. Introduction

Since Fujishima and Honda first discovered the phenomenon of photocatalytic splitting of water with TiO_2 under UV irradiation [1], enormous efforts have been devoted to the research of this material. TiO_2 has many advantageous features, including its low cost, nontoxicity, and high stability, which bestow it with many promising applications in the field of photocatalysis [2–4]. However, the highly efficient use of TiO_2 is sometimes restricted by its wide band gap (3.2 eV for the anatase phase). The band gap lies in the UV regime, which is only a small fraction of the sun's energy [5].

In order to improve the utilization of solar energy, many attempts have been carried out to extend the adsorption of TiO_2 into visible light region. Among these various works, metal ion [6–8] and nonmetal [9–11] doping have been proposed to improve the photocatalytic performance of the TiO_2-based catalysts. However, these doped materials have suffered from low doping concentration and low charge separation efficiency [8,12,13]. Sensitization with functional carbonaceous materials has since proved to be one of the promising strategies that can overcome the drawbacks, in which the C element is always suggested to adhere with TiO_2 via C—O—Ti bonds, thus avoiding carbon from doping directly into the lattice of TiO_2, which decreases the probability of electron/hole recombination. Moreover, modification with carbon can enhance the adsorption capacity of organic compounds, which may promote the removal of organic contaminant from water [14].

On the other hand, the diffusion is also a serious problem that limits the performance of photocatalysts. Fabrication of hollow structures is expected not only to reduce the diffusion length, but also improve the accessibility of active sites to the reactants, resulting in a performance improvement for catalysts [15–17]. Therefore, it appears to be particularly significant for constructing TiO_2/C with hollow structures. Two general methods, template-sacrificial techniques and template-free approaches, have been employed to prepare the inorganic hollow materials [18–23]. In particular, the template method is the most effective and common, especially for the soft templates, which has been successfully used to prepared TiO_2@C hollow microspheres [24]. But these as-prepared hollow products are poor in their morphology and monodispersity and easily collapsed in the process of removing template [25]. Furthermore, as is known, though employing with hard templates (usually SiO_2 and Carbon spheres) can obtain diverse inorganic hollow spheres with well-defined and monodisperse morphology, the removal of the template is very complicated and energy consuming [26]. Yu et al. [27] have reported an interesting spontaneous dissolution approach to synthesis of hierarchically nanoporous TiO_2 hollow microspheres by using TiF_4 as the precursor and SiO_2 microspheres as templates. In the work, the hydrolysis of TiF_4 leads to the production of HF and HF is then used to etch the SiO_2 core. However, the products have only an extremely limited carbon content. And it is still a challenge for preparation of TiO_2@C hollow structure with abundant carbon content through the hard-template method.

In this paper, TiO_2@C hollow composite materials were prepared by combining simple sol–gel and hydrothermal processes.

* Corresponding author. Tel.: +86 25 52090617; fax: +86 25 52090617.
E-mail address: ymzhou@seu.edu.cn (Y. Zhou).

0169-4332/$ – see front matter © 2013 Elsevier B.V. All rights reserved.
http://dx.doi.org/10.1016/j.apsusc.2013.09.084

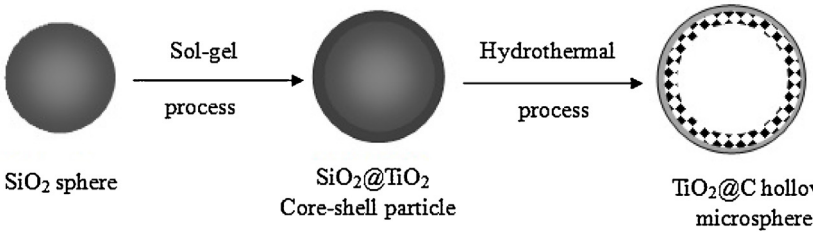

Fig. 1. Schematic illustration of the synthetic procedure used for fabrication of TiO_2@C hollow composite structures.

The SiO_2@TiO_2 core–shell spheres were employed as the hard template for the preparation of TiO_2@C hollow microspheres. SiO_2 core gradually dissolved with the hydrothermal treatment time, thus an extra process, for example etching, was no longer needed to leave behind a hollow shell. It is worthy of note that the spontaneous dissolution of silica core are free from using etching agents, which are hard completely washed away and harmful for the body. More importantly, the dense carbon coating makes it difficult for the etching agents to reach the inner silica core, and thus it is hard to obtain a well-confined hollow spheres without the spontaneous dissolution of silica core. The schematic illustration of the procedure was shown in Fig. 1. By simply tuning the glucose concentration, the thickness of carbon layer could be easily controlled. A possible mechanism for the formation of hollow structure was proposed. The investigation of photocatalytic ability indicated that the as-prepared composite exhibited enhanced photocatalytic performance for the adsorption and decomposition of RhB under visible-light irradiation.

2. Experimental

2.1. Chemicals

Tetraethyl orthosilicate (TEOS), ethanol, concentrated ammonia solution (28 wt%), polyvinylpyrrolidone (M.W. ~ 50,000) and glucose were of analytical grade and tetrabutyl titanate (TBOT) were of chemical grade, all of them were purchased from Sinopharm Chemical Reagent Co., Ltd. Hydroxypropyl cellulose (HPC, M.W. ~ 100,000) were obtained from Alfa Aesar. Rhodamine B (RhB, pure) was purchased from Tianjing Chemical Reagent Research Institute. All chemicals were used as received without further purification. Deionized water was used for all experiments.

2.2. Synthesis of SiO_2 spheres

TEOS (3.44 mL) was mixed with concentrated ammonia solution (4.96 mL), deionized water (34.4 mL) and ethanol (184 mL). The mixture was stirred for 6 h at room temperature, and then the SiO_2 spheres were centrifuged and washed with ethanol, and re-dispersed in ethanol under ultrasonication.

2.3. TiO_2 coating

The above-mentioned SiO_2 suspension was dispersed in a mixture containing HPC (0.8 g), ethanol (200 mL), and de-ionized water (0.8 mL). Then, a stock solution containing TBOT (8 mL) and ethanol (40 mL) was slowly added to the mixture. After injection, the temperature was increased to 85 °C, and the reaction mixture was stirred for 100 min, the SiO_2/TiO_2 colloids were collected by centrifugal separation, washed with ethanol. In order to obtain a thicker TiO_2 layer, the above coating process was repeated and dispersed in water (160 mL).

2.4. Carbon coating

In a typical experiment, 20 mL of the above-mentioned SiO_2/TiO_2 solution was re-dispersed in glucose solution (100 mL). The concentration of glucose (W) varied from 0, 5, 10 to 15 g/L. The mixture was then sealed into a Teflon-lined autoclave, followed by hydrothermal treatment at 180 °C for 16 h in a static state. The resulting brown solid particles were separated, washed and dried.

2.5. Characterization methods

Transmission electron microscopy (TEM) analysis was performed on a JEM-1230 microscope at an accelerating voltage of 100 kV. The samples were prepared by dropping and evaporating particle suspension on to a Cu grid. X-ray diffraction (XRD) data were collected on a Bruck D8 instrument using a Cu Kα radiation source (λ = 1.54056 Å). Fourier transform infrared (FT-IR) spectra were measured on a Nicolet Magna-IR 750 spectrophotometer using KBr pellet in the 4000–400 cm^{-1} range. X-ray photoelectron spectroscopy (XPS) measurements were accomplished in a Thermo ESCALAB 250 instruments (USA) using nonmonochromatic Al Ka ($h\nu$ = 1486.6 ev) radiation. The pressure of the analysis chamber was kept at 4×10^{-10} Torr. Binding energies were referred to the C 1s peak at 284.8 ev. The peak areas were estimated by fitting the experimental results with Lorentzian–Gaussian curves. The nitrogen adsorption–desorption isotherms were measured at −196 °C on a Micromeritics ASAP 2020 apparatus. Before measurements, the samples were degassed at 120 °C and 1×10^{-3} Torr for 12 h. The pore size distribution was analyzed by the Barrett–Joyner–Halenda (BJH) method. The UV-vis diffuse reflectance spectroscopy was carried out on a Shimadzu UV 3600 spectrometer.

2.6. Photocatalytic activity measurement

Photocatalytic activity of the samples was evaluated by degradation of Rhodamine B (RhB) under a 1000 W tungsten lamp equipped with a cutoff filter (λ > 420 nm). To keep the reaction at room temperature, the reaction flask was put in a cooling water system. 50 mg of the catalyst was dispersed in a 50 mL RhB aqueous solution (2×10^{-5} mol/L). Prior to illumination, the suspensions were stirred in dark for 30 min to ensure that RhB was adsorbed to saturation on the surface of catalysts. The concentration of RhB was estimated by measuring the absorbance at their maximum peaks (553 nm) with the Shimadzu UV 3600 spectrometer.

3. Results and discussion

3.1. Morphology and structure of the composite spheres

The notations, the concentration of glucose (W), average spheres size (D), grain size, BET surface area for the samples were summarized in Table 1.

Table 1
Notations, the concentration of glucose (W), average spheres size (D), grain size, and BET surface area of the samples synthesized in this work.

Sample notation	W (g/L)	D (nm)[a]	Grain size (nm)[b]	S_{BET} ($m^2\ g^{-1}$)
SiO_2@TiO_2	–	209	–	205.5
TiO_2/C-W0	0	211	17.4	70.4
TiO_2/C-W5	5	215	12.6	58.8
TiO_2/C-W10	10	223	12.7	26.6
TiO_2/C-W15	15	257	12.3	4.6

[a] Calculated from more than 100 particles in the corresponding TEM image.
[b] Determined by XRD using the Scherrer equation.

X-ray diffraction (XRD) was carried out to investigate the phase structure and crystallite size of the as-prepared samples. As shown in Fig. 2a, the as-prepared SiO_2@TiO_2 core–shell composite particles showed a broad peak between 20° and 30°, which was the background peak attributed to the glass slide. No other peaks were observed, indicating that SiO_2@TiO_2 was amorphous phase. TiO_2/C hollow spheres were prepared by hydrothermal treatment of SiO_2@TiO_2 spheres with different concentration of glucose (W = 0, 5, 10 and 15 g/L). The related XRD patterns were shown in Fig. 2b–d. As observed in Fig. 2b, the diffraction peaks appeared at 2θ = 25.4° (1 0 1), 37.9° (0 0 4), 48.0° (2 0 0), 53.8° (1 0 5), 54.9° (2 1 1) and 62.8° (2 0 4) were attributed to the anatase TiO_2 (JCPDS, No. 21-1272) and the diffraction peak appeared at 2θ = 30.7° was attributed to brookite TiO_2 (JPCDS No. 29-1360), which revealed that a trace amount of brookite phase coexisted with anatase phase for the sample prepared in the absence of glucose (W = 0). While in the presence of glucose, the diffraction peak of brookite disappeared, indicating that carbon coating inhibited the formation of brookite phase. Furthermore, it was found that the XRD intensity decreased with the carbon coating by comparing the (1 0 1) peak, which may arise from the shield effect of the carbon species [28]. The average crystal sizes of the TiO_2 were estimated by applying the Debye-Scherrer formula and were listed in Table 1. It could be seen that the average grain sizes of TiO_2 crystallites were about 12.5 nm for all the TiO_2/C composite spheres.

The morphology and structure of the samples were investigated by transmission electron microscopy (TEM). As shown in Fig. 3a, the SiO_2@TiO_2 samples prepared through sol–gel methods were well-defined solid spheres with a ~6 nm thick amorphous TiO_2 shell. After hydrothermal treatment of the core–shell spheres for 16 h in pure water (W = 0), most of the particles were still solid spheres but with rough surfaces (Fig. 3b), indicating the crystallization of TiO_2 shell. However, quantities of the TiO_2 particles escaped from the silica surface and gathered into large aggregates of irregular shapes, which may be due to the extensive grain growth. While in the presence of glucose, no aggregates of TiO_2 particles outside the composite structure were observed in the TEM images. The surface of spheres was smooth, indicating the presence of a layer of carbon covering on the TiO_2 surface after hydrothermal reaction. It was possible that the deposited carbon on the TiO_2 surface may act as barriers against the structure rearrangement in TiO_2 shell. Further observation of the TiO_2 layer revealed that the TiO_2 particles size was about 12 nm, which was in good agreement with the XRD results. Besides, the thickness of carbon layer could be well controlled by simply changing the concentration of glucose (Fig. S1). For all the carbon coated composite spheres, hollow structure was obtained, as evidenced by the intensive contrast between the dark edge and the pale center. In the hydrothermal procedure, the SiO_2 core was removed spontaneously. Thus an additional process was no longer required to remove them.

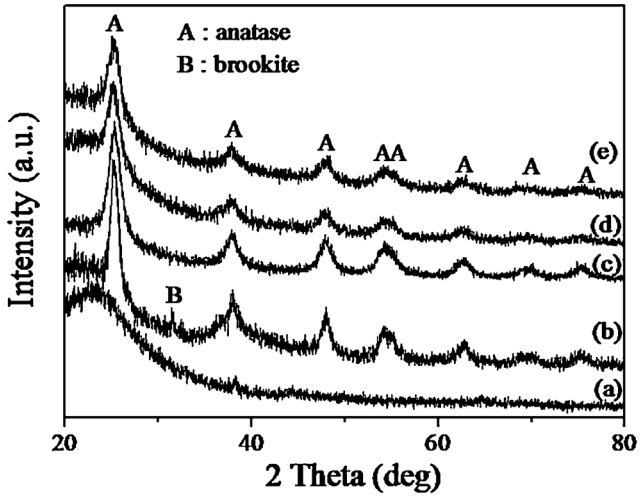

Fig. 2. XRD patterns of the SiO_2@TiO_2 sample (a) and the TiO_2/C samples prepared at W = 0 (b), 5 (c), 10 (d), and 15 (e), respectively.

3.2. Formation mechanism

The possible formation mechanism of the hollow spheres was investigated by the time-dependent evolution experiments, in which the concentration of glucose was fixed while the time of the hydrothermal reaction was varied from 4 h to 18 h. The morphology evolution of the corresponding samples was investigated by TEM studies. Prior to the reaction (0 h), the sample was solid spheres with a smooth surface (Fig. 4a). After hydrothermal treatment for 4 h, the surface of the sample became obviously rough, indicating the formation of crystalline TiO_2 particles (Fig. 4b). At the time, the product was still solid spheres without carbon coated on the surface. Extending the reaction time to 8 h, the surface of the sample was slightly smooth, demonstrating that the carbon species were started to incorporate into the composite structure (Fig. 4c). Besides, the hollow interiors appeared around the center of the solid spheres. The pH of the solution was ~3 while the pH of the solution without the addition of glucose was ~7, the acidic environment should be attributed to the carbonization of glucose under the hydrothermal conditions. In general, SiO_2 is remarkably stable in a normal acidity solution. In the high-pressure environment, H_2O can serve as the etching agent and induce the dissolution of silica in the solution [29]. SiO_2 may gradually translate to $Si(OH)_4$, which was soluble during the hydrothermal treatment, for the out of the dissolving equilibrium of $Si(OH)_4$ in the reaction solution. In our system, the H^+ in the solution may accelerate the dissolving of SiO_2 by react with $Si(OH)_4$ to form Si^{4+}. Moreover, the HPC, which was used as the surfactant for preparing TiO_2 shell [30,31], was absorbed to the surface of SiO_2 core. The tight connection between HPC and SiO_2 (through hydrogen bonds) may effectively protect the surface of SiO_2 core from rapid dissolution. What is more, the composite spheres were porous and had large specific surface areas, both for the precursor colloidal oxides and the products

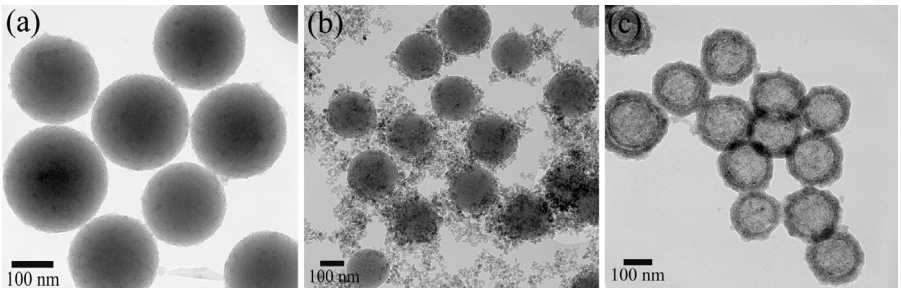

Fig. 3. TEM images of (a) SiO_2/TiO_2, (b) TiO_2/C-W0, and (c) TiO_2/C-W10.

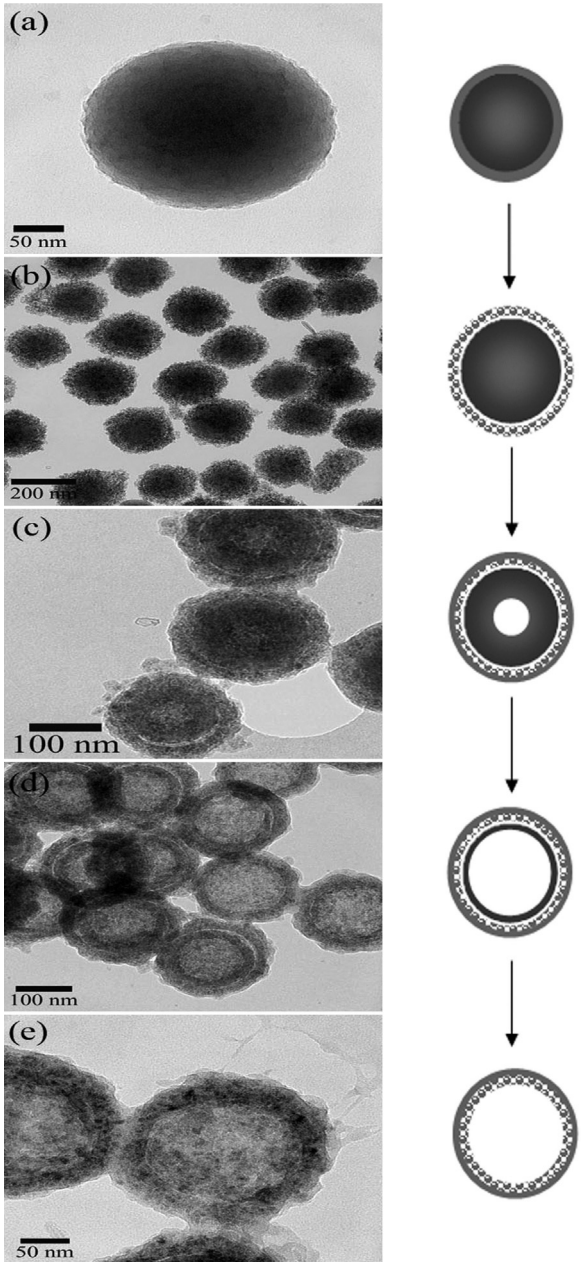

Fig. 4. Left, TEM images showing the morphology and structure evolution of SiO_2@TiO_2 samples after hydrothermal treatment in the presence of glucose for different time periods: (a) 0 min, (b) 4 h, (c) 8 h, (d) 12 h and (e) 16 h. Right, the corresponding schematic illustration of each step.

(see Table 1). Therefore, Si^{4+} can easily transfer from the center of the spheres to the outside solution, resulting in a hollow space occurring first at the center of the core. It was noteworthy that the hydrogen bonds suppressed the carbonization of HPC, thus HPC was relatively stable in this stage. Further increasing the reaction time to 12 h, the hollow core expanded outward with the growth of the carbon layer (Fig. 4d). After reaction for 16 h, the carbon layer increased to ~5 nm and hollow microspheres were finally obtained (Fig. 4e). With extending the hydrothermal treatment time, the hollow space was gradually growing outward until the core dissolved completely. This method can be considered as the self-templating method [32], typically the surface-protected etching [31].

XRD was also applied to investigate the crystallization process of TiO_2. As shown in Fig. S2, all the intermediate products exhibited only the characteristic peaks of anatase phase. After hydrothermal treatment for 4 h, the diffraction peaks was relatively sharp and intense, indicating the highly crystalline TiO_2 particles. It should be noteworthy that little change in the diffraction peaks was detected with the further extending the reaction time, apparently due to the deposition of the carbon barrier that prevented the further crystal growth of TiO_2 particles. The carbon layer also prevented the structure reconstruction of the TiO_2 shells, resulting in well-defined hollow spheres.

3.3. Porosity characteristics, chemical environment and optical properties

Fig. 5 shows the nitrogen adsorption–desorption isotherm and the corresponding pore size distribution curve (inset) of the sample obtained at $W = 10$ for representation. The hollow sample exhibited a Type IV absorption isotherms with a H3 hysteresis loop [33] indicating the mesoporous characteristics. The sharp peak around

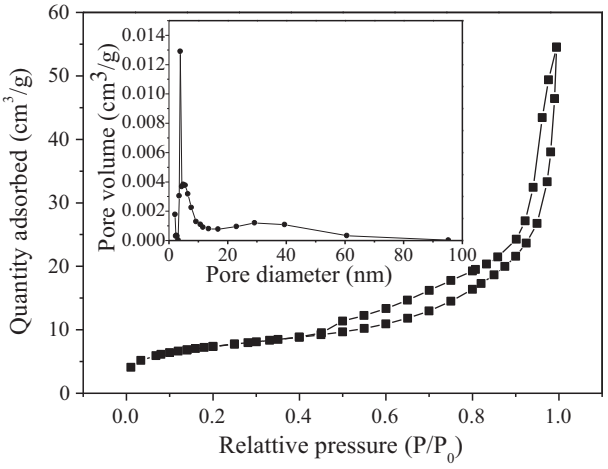

Fig. 5. N_2 adsorption–desorption isotherm and corresponding pore size distribution curve (inset) of the hollow TiO_2/C microspheres prepared at $W = 10$.

3.8 nm in the BJH pore size distribution analysis revealed a relatively narrow pore size distribution. However, the reference sample prepared at $W = 0$ showed a broad pore size distribution centered around 11 nm (Fig. S3), which may be attributed to the uncontrolled growth of TiO_2 crystallite. Table 1 listed the BET surface areas of the samples synthesized herein. The pristine amorphous SiO_2@TiO_2 had the largest BET surface area. With increasing W (from 0 to 15), the samples showed a monotonic decrease in specific surface areas, apparently because the carbon that incorporated into the products blocked some pores and channels.

Thermogravimetric analysis (TGA) was carried out to calculate the C content in the composite spheres. Fig. S5 showed the TGA curve for the TiO_2/C-W10. Heating the composite particles in an air flow to 800 °C led to two main weight losses. The one that occurred between 50 °C and 250 °C with a weight loss of about 6.2% could be attributed to the desorption of adsorbed water from the TiO_2/carbon samples, and the second weight loss of about 24.1%, which occurred between 250 °C and 600 °C, might be resulted from the combustion of the carbon layer and the surfactants (HPC) in air. Furthermore, the burning of the carbon species burst at only 250 °C, which suggested that most the carbon element was not likely to be doped directly into the TiO_2 lattice [34,35]. Once the carbon element was doped into the TiO_2 lattice, more energy was needed to destroy the interaction between TiO_2 and carbon [36]. In the FTIR spectra (Fig. S4(b)), the presence of carbon layer on the TiO_2 surface was also demonstrated with a significant enhanced absorption peak at ~3100 cm^{-1}, which was related to the stretching vibration C—H in aromatic ring. The aromatic ring is one of the dehydration products of the hydrothermal carbonization of glucose and serves as building blocks for the construction of the carbon layer [37].

X-ray photoelectron spectroscopy (XPS) was carried out to further investigate the chemical and bonding environment of the TiO_2 and carbon. As observed in Fig. 6a, the fully scanned spectrum demonstrated that Ti, C, and O elements existed in the TiO_2/C composite spheres (W10). Fig. 6b showed the high resolution XPS spectra of the Ti 2p peak. It could be seen from the spectra that two peaks occurred at 464.8 eV and 458.9 eV were corresponded to the Ti $2p_{1/2}$ and Ti $2p_{3/2}$ binding energies, respectively. The splitting of the Ti 2p doublet was 5.9 eV, indicating a normal state of Ti^{4+} in the TiO_2@C-W10 sample [38]. The C 1s spectra exhibited a wide and asymmetric peak centered at 285 eV, suggesting that several kinds of carbon coexisted (Fig. 6c). The main C 1s peak was dominated by elemental carbon at 284.6 eV, attributed mainly to sp^2 hybridized carbon [39]. Two peaks at 285.9 and 288 eV were characteristic of the oxygen bound species C—O and C═O, respectively [40,41]. According to the literature [42,43], the C 1s peak at 281 eV should be observed if the C element existed in the form of doping and which was assigned to the C substituting oxygen element in the lattice of TiO_2 (Ti—C bond). In our experiment, no C 1s peak at 281 eV was seen in the XPS pattern, indicating that the carbon atom did not enter the TiO_2 lattice. The absence of Ti—C bonds (C doping) may be attributed to the mild hydrothermal environment and the pre-built TiO_2 precursor, which highly confined the form of C doped TiO_2. Fig. 6d presented the spectra of O 1s for the TiO_2/C-W10 sample. The peaks at 529.8 eV, 531.2 eV, 532.4 eV, and 533.4 eV were attributed to Ti—O—Ti (lattice O), surface hydroxyl groups (O—H), oxygen in the C—O—Ti bond and oxygen making a double bond with carbon (C═O), respectively [44,45]. On the basis of these observations, it is inferred that the carbon layer is covered on the TiO_2 surface and combined with TiO_2 via C—O—Ti bonds. It should be illustrated that the Ti—O—C bond will benefit to the charge transfer between TiO_2 and C layer upon light excitation, and thus facilitate the interface reaction of photocatalysis.

The UV–vis diffuse reflectance spectra of the as-prepared samples were shown in Fig. 7. The pure TiO_2 sample (prepare at $W = 0$) had no absorption in the visible region (>400 nm). While for the TiO_2/C samples, the curves showed significant enhancement of light absorption in the range of 400–800 nm. The remarkable light absorption in the visible region of these hybrid samples was attributed to the incorporation of carbon into the final products, because carbon had the capability of absorbing visible light [46]. Notable, the absorption band edge of TiO_2 was also changed with

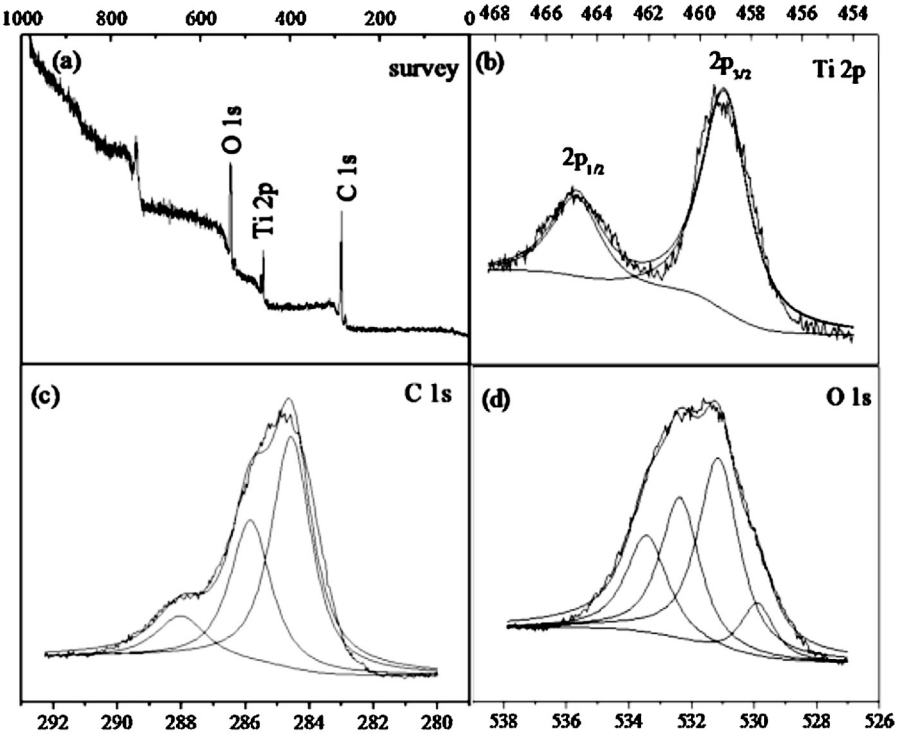

Fig. 6. XPS spectra of the TiO_2/C-W10 for representation: fully scanned spectrum (a), fitting spectra of Ti 2p (b), C 1s (c) and O1s (d).

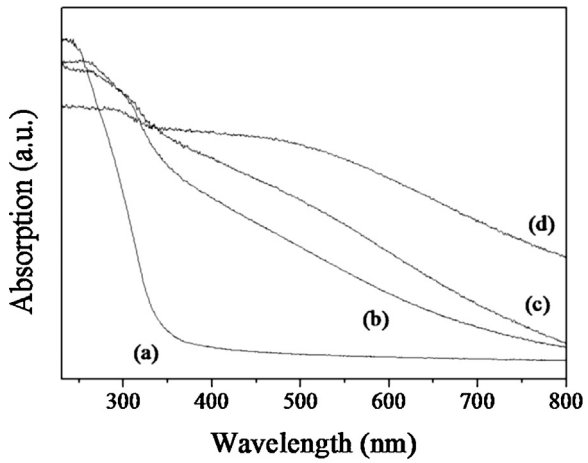

Fig. 7. UV–vis diffuse reflectance spectra of the samples prepared at $W = 0$ (a), $W = 5$ (b), $W = 10$ (c), and $W = 15$ (d).

the carbon content and this variation increased with carbon content of the TiO_2/C samples, demonstrating that an increase of surface electric charge in the samples [47]. The joint electronic system formed between carbon and TiO_2 may give rise in synergistic properties and enhance the photocatalytic activity.

3.4. Photocatalytic activity

The photocatalytic activities of the as-prepared samples were evaluated by the degradation of Rhodamine B (RhB) under visible light irradiation and shown in Fig. 8. In the experiments, the pure TiO_2 sample ($W = 0$) was used as the photocatalytic references and the degradation efficiency of the samples was defined as C/C_0, where C and C_0 stood for the remnants and initial concentration of RhB, respectively. Before the light irradiation, the mixtures containing the catalysts and RhB were stirred in the dark for 30 min to ensure that the adsorption–desorption equilibrium of RhB was estabilished, and the adsorption efficiencies of W0, W5, W10 and W15 were 4.1%, 42.3%, 39.0% and 23.4%, respectively. Compared with the pure TiO_2 sample (W0), all the carbon composite samples exhibited high adsorption ability for RhB. The enhanced adsorption of organic contaminants may be due to the carbonaceous polymer [24], which has abundant functional groups to adsorb organic dyes. The adsorption of RhB slightly decreased with the increasing of glucose content from 5 g/L to 10 g/L, and dramatically decreased when

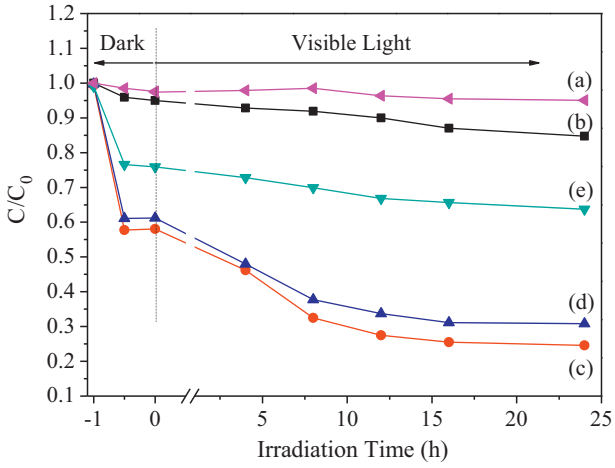

Fig. 8. Degradation profiles of RhB in the presence of different TiO_2/C catalysts. (a) Blank experiment, (b) W0, (c) W5, (d) W10 and (e) W15.

the glucose content increased to 15 g/L. The excess carbon deposition leads to a loss of surface area, resulting in less active sites for absorbing the organic dye.

In the blank test (no photocatalyst), no appreciable degradation of RhB was observed after visible-light irradiation for 24 h, while the photodegradation rate was significantly enhanced in the presence of catalysts, especially for the TiO_2/C-W5 sample, which showed highest catalytic efficiencies. TiO_2/C-W10 sample showed a comparable catalytic activity toward the degradation of RhB. We suggest that both the carbon content and surface area contribute a lot to the degradation reaction. As observed in Fig. 7, increasing carbon content in the composite spheres promotes the adsorption of visible light and thus facilitates the generation of electrons (e^-). However, with the carbon content increased, the surface area decreased, resulting in a loss of the diffusion rate of RhB to the surface of TiO_2. Therefore, the TiO_2/C-W15, which had the highest carbon content but exhibited the lowest photocatalytic activity among the TiO_2/C composite samples. Moreover, it should be underlined that the hollow structure also contributed a lot to its higher photocatalytic properties. The hollow TiO_2/C samples possessed high specific surface area and rich pores, thus the mass transfer of dye molecules was facilitated, resulting in an enhanced photodegradation activity. Besides, it was noteworthy that the photocatalytic degradation of RhB molecules proceeded to a certain extent for the pure TiO_2 (W0) under the visible light irradiation, though the TiO_2/C-W0 had no absorption in visible light. In this case, the photodegradation of RhB was usually suggested to be caused by the self-photosensitized transformation of RhB molecules over TiO_2 semiconductor [48,49].

On the basis of the above experimental results and discussion, a possible photocatalytic mechanism was proposed as well. As reported before [50], the sensitizers can be excited by visible light to generate charge, which is then injected into the conduction band of TiO_2 to initiate the photodegradation reaction. In our work, similarly, both the carbon and the organic dye could be served as the sensitizers and transferred electrons to the conductive band of TiO_2. Then, dissolved oxygen molecules (O_2) may accept the electrons and form superoxide radical anions ($\bullet O_2^-$), which then oxidizes RhB directly on the surface of TiO_2 or produces hydroperoxy radicals ($HO_2\bullet$) and hydroxyl radicals ($OH\bullet$) by protonation prior to oxidize the organic dyes.

4. Conclusions

In summary, with the TiO_2@SiO_2 core–shell spheres as the raw material, mesoporous TiO_2/C hollow spheres have been prepared by a facile hydrothermal method. The formation of the hollow structure is via a spontaneous dissolution of SiO_2 cores in the hydrothermal process and does not require a traditional etching approach to remove them. The dissolution initially forms centered hollow space, and eventually removes the core material to leave behind the hollow composite spheres. The combined carbon can extend the photoresponse of TiO_2 to the visible region, and promote the performance in the adsorption and decomposition of RhB under visible light irradiation.

Acknowledgements

The authors are grateful to the financial supports of National Natural Science Foundation of China (Grant No. 21376051, 21306023, 21106017 and 51077013), Natural Science Foundation of Jiangsu (Grant No. BK20131288), Fund Project for Transformation of Scientific and Technological Achievements of Jiangsu Province of China (Grant No. BA2011086), Specialized Research Fund for the Doctoral Program of Higher Education of China (Grant No. 20100092120047), Key Program for the Scientific Research

Guiding Found of Basic Scientific Research Operation Expenditure of Southeast University (Grant No. 3207043101) and Instrumental Analysis Fund of Southeast University.

Appendix A. Supplementary data

Supplementary data associated with this article can be found, in the online version, at http://dx.doi.org/10.1016/j.apsusc.2013.09.084.

References

[1] A. Fujishima, K. Honda, Electrochemical photolysis of water at a semiconductor electrode, Nature 238 (1972) 37–38.
[2] S.U.M. Khan, M. Al-Shahry, W.B. Ingler, Efficient photochemical water splitting by a chemically modified n-TiO_2, Science 297 (2002) 2243–2245.
[3] P.V. Kamat, Photochemistry on nonreactive and reactive (semiconductor) surfaces, Chem. Rev. 93 (1993) 267–300.
[4] M.R. Hoffmann, S.T. Martin, W.Y. Choi, D.W. Bahnemann, Environmental applications of semiconductor photocatalysis, Chem. Rev. 95 (1995) 69–96.
[5] A.L. Linsebigler, G.Q. Lu, J.T. Yates, Photocatalysis on TiO_2 surfaces – principles, mechanisms, and selected results, Chem. Rev. 95 (1995) 735–758.
[6] M. Anpo, M. Takeuchi, The design and development of highly reactive titanium oxide photocatalysts operating under visible light irradiation, J. Catal. 216 (2003) 505–516.
[7] J. Arana, O.G. Diaz, M.M. Saracho, J.M.D. Rodriguez, J.A.H. Melian, J.P. Pena, Photocatalytic degradation of formic acid using Fe/TiO_2 catalysts: the role of Fe^{3+}/Fe^{2+} ions in the degradation mechanism, Appl. Catal. B-Environ. 32 (2001) 49–61.
[8] W.Y. Choi, A. Termin, M.R. Hoffmann, The role of metal-ion dopants in quantum-sized TiO_2-correlation between photoreactivity and charge–carrier recombination dynamics, J. Phys. Chem. 98 (1994) 13669–13679.
[9] X.B. Chen, L. Liu, P.Y. Yu, S.S. Mao, Increasing solar absorption for photocatalysis with black hydrogenated titanium dioxide nanocrystals, Science 331 (2011) 746–750.
[10] J.W. Wang, B.D. Mao, J.L. Gole, C. Burda, Visible-light-driven reversible and switchable hydrophobic to hydrophilic nitrogen-doped titania surfaces: correlation with photocatalysis, Nanoscale 2 (2010) 2257–2261.
[11] S. In, A. Orlov, R. Berg, F. Garcia, S. Pedrosa-Jimenez, M.S. Tikhov, D.S. Wright, R.M. Lambert, Effective visible light-activated B-doped and B,N-codoped TiO_2 photocatalysts, J. Am. Chem. Soc. 129 (2007) 13790–13791.
[12] J. Graciani, L.J. Alvarez, J.A. Rodriguez, J.F. Sanz, N doping of rutile TiO_2 (110) surface. A theoretical DFT study, J. Phys. Chem. C 112 (2008) 2624–2631.
[13] R. Asahi, T. Morikawa, T. Ohwaki, K. Aoki, Y. Taga, Visible-light photocatalysis in nitrogen-doped titanium oxides, Science 293 (2001) 269–271.
[14] X. Chen, S.S. Mao, Titanium dioxide nanomaterials: synthesis, properties, modifications, and applications, Chem. Rev. 107 (2007) 2891–2959.
[15] J.B. Joo, Q. Zhang, I. Lee, M. Dahl, F. Zaera, Y.D. Yin, Mesoporous anatase titania hollow nanostructures though silica-protected calcination, Adv. Funct. Mater. 22 (2012) 166–174.
[16] K.L. Lv, B. Cheng, J.G. Yu, G. Liu, Fluorine ions-mediated morphology control of anatase TiO_2 with enhanced photocatalytic activity, Phys. Chem. Chem. Phys. 14 (2012) 5349–5362.
[17] J.N. Liu, G.W. Zhang, W. Ao, K. Yang, S.X. Peng, C. Muller-Goymann., Hollow mesoporous titania microsphere with low shell thickness/diameter ratio and high photocatalysis, Appl. Surf. Sci. 258 (2012) 8083–8089.
[18] F. Caruso, R.A. Caruso, H. Mohwald, Nanoengineering of inorganic and hybrid hollow spheres by colloidal templating, Science 282 (1998) 1111–1114.
[19] X. Wu, G.Q. Lu, L.Z. Wang, Shell-in-shell TiO_2 hollow spheres synthesized by one-pot hydrothermal method for dye-sensitized solar cell application, Energy Environ. Sci. 4 (2011) 3565–3572.
[20] X.W. Lou, L.A. Archer, Z.C. Yang, Hollow micro-/nanostructures: synthesis and applications, Adv. Mater. 20 (2008) 3987–4019.
[21] T.H. Kim, K.H. Lee, Y.K. Kwon, Monodisperse hollow titania nanospheres prepared using a cationic colloidal template, J. Colloid Interf. Sci. 304 (2006) 370–377.
[22] J.G. Yu, J. Zhang, A simple template-free approach to TiO_2 hollow spheres with enhanced photocatalytic activity, Dalton Trans. 39 (2010) 5860–5867.
[23] X.L. Wang, H.L. He, Y. Chen, J.Q. Zhao, X.Y. Zhang, Anatase TiO_2 hollow microspheres with exposed {0 0 1} facets: facile synthesis and enhanced photocatalysis, Appl. Surf. Sci. 258 (2012) 5863–5868.
[24] J.D. Zhuang, Q.F. Tian, H. Zhou, Q. Liu, P. Liu, H.M. Zhong, Hierarchical porous TiO_2@C hollow microspheres: one-pot synthesis and enhanced visible-light photocatalysis, J. Mater. Chem. 22 (2012) 7036–7042.
[25] J. Hu, M. Chen, X.S. Fang, L.W. Wu, Fabrication and application of inorganic hollow spheres, Chem. Soc. Rev. 40 (2011) 5472–5491.
[26] X.P. Lin, D.M. Song, X.Q. Gu, Y.L. Zhao, Y.H. Qiang, Synthesis of hollow spherical TiO_2 for dye-sensitized solar cells with enhanced performance, Appl. Surf. Sci. 263 (2012) 816–820.
[27] J.G. Yu, W. Liu, H.G. Yu, A one-pot approach to hierarchically nanoporous titania hollow microspheres with high photocatalytic activity, Cryst. Growth Des. 8 (2008) 930–934.
[28] W.J. Ren, Z.H. Ai, F.L. Jia, L.Z. Zhang, X.X. Fan, Z.G. Zou, Low temperature preparation and visible light photocatalytic activity of mesoporous carbon-doped crystalline TiO_2, Appl. Catal. B-Environ. 69 (2007) 138–144.
[29] Q.Y. Yu, P.P. Wang, S. Hu, J.F. Hui, J. Zhuang, X. Wang, Hydrothermal synthesis of hollow silica spheres under acidic conditions, Langmuir 27 (2011) 7185–7191.
[30] M.M. Ye, Q. Zhang, Y.X. Hu, J.P. Ge, Z.D. Lu, L. He, Z.L. Chen, Y.D. Yin, Magnetically recoverable core–shell nanocomposites with enhanced photocatalytic activity, Chem. Eur. J. 16 (2010) 6243–6250.
[31] Q. Zhang, I. Lee, J.P. Ge, F. Zaera, Y.D. Yin, Surface-protected etching of mesoporous oxide shells for the stabilization of metal nanocatalysts, Adv. Funct. Mater. 20 (2010) 2201–2214.
[32] X.L. Fang, X.J. Zhao, W.J. Fang, C. Chen, N.F. Zheng, Self-templating synthesis of hollow mesoporous silica and their applications in catalysis and drug delivery, Nanoscale 5 (2013) 2205–2218.
[33] K.S.W. Sing, D.H. Everett, R.A.W. Haul, L. Moscou, R.A. Pierotti, J. Rouquerol, T. Siemieniewska, Reporting physisorption data for gas solid systems with special reference to the determination of surface-area and porosity (Recommendations 1984), Pure Appl. Chem. 57 (1985) 603–619.
[34] J. Zhong, F. Chen, J.L. Zhang, Carbon-deposited TiO_2: synthesis, characterization, and visible photocatalytic performance, J. Phys. Chem. C 114 (2010) 933–939.
[35] P. Zhang, C.L. Shao, Z.Y. Zhang, M.Y. Zhang, J.B. Mu, Z.C. Guo, Y.C. Liu, TiO_2@carbon core/shell nanofibers: controllable preparation and enhanced visible photocatalytic properties, Nanoscale 3 (2011) 2943–2949.
[36] T. Yu, Y.H. Deng, L. Wang, R.L. Liu, L.J. Zhang, B. Tu, D.Y. Zhao, Ordered mesoporous nanocrystalline titanium-carbide/carbon composites from in situ carbothermal reduction, Adv. Mater. 19 (2007) 2301–2306.
[37] X.M. Sun, Y.D. Li, Colloidal carbon spheres and their core/shell structures with noble-metal nanoparticles, Angew. Chem. Int. Ed. 43 (2004) 597–601.
[38] P. Zhang, C.L. Shao, Z.Y. Zhang, M.Y. Zhang, J.B. Mu, Z.C. Guo, Y.Y. Sun, Y.C. Liu, Core/shell nanofibers of TiO_2@carbon embedded by Ag nanoparticles with enhanced visible photocatalytic activity, J. Mater. Chem. 21 (2011) 17746–17753.
[39] L. Zhao, X.F. Chen, X.C. Wang, Y.J. Zhang, W. Wei, Y.H. Sun, M. Antonietti, M.M. Titirici, One-step solvothermal synthesis of a carbon@TiO_2 Dyade structure effectively promoting visible-light photocatalysis, Adv. Mater. 22 (2010) 3317–3321.
[40] Z.S. Dai, F.H. Shi, B.Y. Zhang, M. Li, Z.G. Zhang, Effect of sizing on carbon fiber surface properties and fibers/epoxy interfacial adhesion, Appl. Surf. Sci. 258 (2011) 1894.
[41] F. Ahimou, C.J.P. Boonaert, Y. Adriaensen, P. Jacques, P. Thonart, M. Paquot, P.G. Rouxhet, XPS analysis of chemical functions at the surface of *Bacillus subtilis*, J. Colloid Interf. Sci. 309 (2007) 49–55.
[42] J.G. Yu, G.P. Dai, Q.J. Xiang, M. Jaroniec, Fabrication and enhanced visible-light photocatalytic activity of carbon self-doped TiO_2 sheets with exposed {0 0 1} facets, J. Mater. Chem. 21 (2011) 1049–1057.
[43] F. Dong, S. Guo, H. Wang, X.F. Li, Z.B. Wu, Enhancement of the visible light photocatalytic activity of C-doped TiO_2 nanomaterials prepared by a green synthetic approach, J. Phys. Chem. C 115 (2011) 13285–13292.
[44] K. Roodenko, M. Gensch, J. Rappich, K. Hinrichs, N. Esser, R. Hunger, Time-resolved synchrotron XPS monitoring of irradiation-induced nitrobenzene reduction for chemical lithography, J. Phys. Chem. B 111 (2007) 7541–7549.
[45] N.P. Zschoerper, V. Katzenmaier, U. Vohrer, M. Haupt, C. Oehr, T. Hirth, Analytical investigation of the composition of plasma-induced functional groups on carbon nanotube sheets, Carbon 47 (2009) 2174–2185.
[46] C. Lettmann, K. Hildenbrand, H. Kisch, W. Macyk, W.F. Maier, Visible light photodegradation of 4-chlorophenol with a coke-containing titanium dioxide photocatalyst, Appl. Catal. B-Environ. 32 (2001) 215–227.
[47] W.D. Wang, C.G. Silva, J.L. Faria, Photocatalytic degradation of Chromotrope 2R using nanocrystalline TiO_2/activated-carbon composite catalysts, Appl. Catal. B-Environ. 70 (2007) 470–478.
[48] T.X. Wu, G.M. Liu, J.C. Zhao, H. Hidaka, N. Serpone, Photoassisted degradation of dye pollutants. V. Self-photosensitized oxidative transformation of Rhodamine B under visible light irradiation in aqueous TiO_2 dispersions, J. Phys. Chem. B 102 (1998) 5845–5851.
[49] S. Cho, J.W. Jang, S. Hwang, J.S. Lee, S. Kim, Self-assembled gold nanoparticle-mixed metal oxide nanocomposites for self-sensitized dye degradation under visible light irradiation, Langmuir 28 (2012) 17530–17536.
[50] L.W. Zhang, H.B. Fu, Y.F. Zhu, Efficient TiO_2 photocatalysts from surface hybridization of TiO_2 particles with graphite-like carbon, Adv. Funct. Mater. 18 (2008) 2180–2189.